

A novel parallel-stranded DNA helix with non canonical A-T and G-C base pairing in synthetic dodecamers

Tapas Saha and Kunal B. Roy*

Centre for Biotechnology, Jawaharlal Nehru University, New Delhi 110 067, India

Interaction between two synthetic deoxyoligonucleotide dodecamers of the same sequence (AGATCTAGATCT) but with reverse polarity at pH 5.2 was studied by UV and CD spectroscopy. UV mixing curve demonstrates formation of 1 : 1 complex between the two dodecamers, which can only be a parallel-stranded DNA (PS-DNA) structure. UV melting curve and CD spectral data are consistent with this view. The PS-DNA possibly form at pH 5.2 by reverse Watson–Crick A-T base pairs and reverse Hoogsteen G-C⁺ base pairs in the same DNA helix. This is the first report of such a novel structure.

DNA oligonucleotides with appropriate sequences can form a stable duplex with the two strands in parallel orientation (PS-DNA), instead of the conventional antiparallel Watson–Crick duplex (APS-DNA)¹. The thermodynamic stability of PS-DNA when formed exclusively with A-T base pairs, is only slightly lower than that of APS-DNA², but incorporation of G-C pairs in such PS-DNA largely destabilizes them³. Numerous studies on spectroscopy, drug-binding⁴, substrate properties^{5,6}, chemical reactivities⁷ and other features of this novel structure have been reported. In these PS-DNA, base pairing is non-canonical (reverse Watson–Crick or Donohue base pairs) with the glycosidic bonds in *trans* orientation and the two grooves are equivalent⁸. Recently, Liu *et al.*⁹ showed that a parallel double helix with Hoogsteen base pairing can exist independently of the triple helix of which it is a component part. The latter PS-DNA consisting of both A-T and G-C base pairs is stable at pH 5.2 but reverts to an imperfect Watson–Crick duplex with loops and mismatches at pH 6.0 and above, despite having perfectly matched sequence of the two strands for Hoogsteen pairing. PS-DNA with exclusively A-T base pairs also undergoes polarity reversal to imperfectly matched APS-DNA upon interaction with drugs like distamycin and netropsin¹⁰. Synthetic oligonucleotides with G-A repeats¹¹ and GGA repeats¹² have also been shown to self-associate to PS-DNA homoduplex with G^{syn}–G^{syn} and A^{anti}–A^{anti} base pairs, which is stable over pH 4–9. Studies to date thus seem to suggest that PS-DNA is severely constrained in the choice of base sequence and composition and requires either a PolyPu.PolyPy sequence (with Hoogsteen pairing) or exclusively A-T base pairs (with Donohue pairing). A schematic comparison of Watson–Crick, reverse Watson–Crick, Hoogsteen bonding

and reverse Hoogsteen bonding are given in Figure 1.

We synthesized two dodecamers 5' d-(AGATCTAGATCT)-3' (RY12), and 5' d-(TCTAGATCTAGA)-3' (YR12) whose sequences are same but of reverse polarity. These are neither PolyPu.PolyPy sequences nor exclusively made of A-T base pairs. These sequences have blocks of three purines and three pyrimidines, and are known to form a triplex by alternate strand recognition¹³. Because of their palindromic nature each of them can form normal Watson–Crick antiparallel duplex in solution. When we study their interaction by UV and CD spectroscopy, we find that YR12 and RY12 can form a parallel duplex or a triplex with alternate strand pairing when mixed in 1 : 1 or 1 : 2 molar ratios, respectively. However, the triplex does not form when YR12 and RY12 are mixed in a ratio of 2 : 1. This is the first report of a parallel duplex with mixed sequence not by Hoogsteen bond alone (although sequences are perfectly matched for it), but possibly with reverse Watson–Crick A-T base pairs.

Synthesis of YR12 and RY12 oligonucleotides was done by solid phase β -cyanoethyl phosphoramidite chemistry¹⁴, using automated DNA synthesizer (Pharmacia Biotech, Gene Assembler Special). Phosphoramidites were from Cruachem, UK. Deprotection and purification of the dodecamer oligonucleotides was done by standard

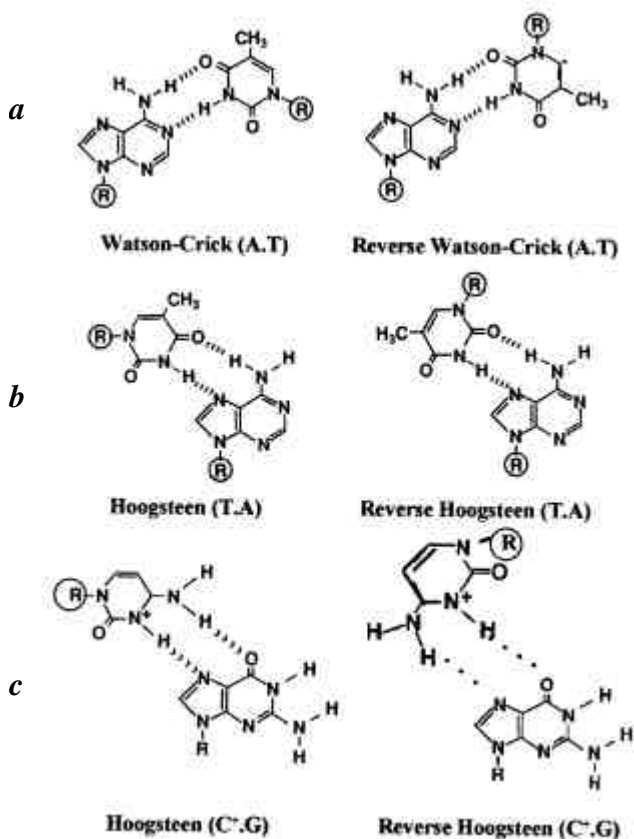


Figure 1. Schematic representations. *a*, Watson–Crick and reverse Watson–Crick base pairing (A-T); *b*, Hoogsteen and reverse Hoogsteen base pairing (A-T); *c*, Hoogsteen and reverse Hoogsteen base pairing (G-C⁺).

*For correspondence. (e-mail: kbroy@jnuniv.ernet.in)

procedure^{15,16}. Purification of oligonucleotides was done by gel electrophoresis using 20% denaturing PAGE followed by desalting on Nap 10 gel filtration column (Pharmacia). The chain length and purity of each oligonucleotide was verified by gel electrophoresis of radiolabelled oligomer. Extinction coefficients of RY12 and YR12 were taken as 9000 M^{-1} in 10 mM NaOH solution (pH 12.0) to determine the concentration.

Thermal denaturation studies were performed using CECIL 599S UV/VIS spectrophotometer with a water-jacketed cell holder connected to a Haake P3 water bath at heating and cooling rates of $0.5^\circ\text{C}/\text{min}$. The thermal transitions were recorded in the range 0°C to 90°C using stoppered cuvette. Solutions of the oligonucleotides were prepared in 10 mM Na-Cacodylate, 300 mM NaCl and 10 mM MgCl_2 (pH 5.2) in appropriate concentration (4.5×10^{-5} – 5.5×10^{-5} M). Prior to melting studies of the oligomer mixtures, solutions were heated to 90°C for two minutes, and then slowly annealed to 0°C . We found heating at 90°C and subsequent slow annealing facilitated formation of the interactive complex fully and resulted in a well-defined melting profile. In the low temperature range (less than 20°C), P_2O_5 and dry N_2 gas were used in the sample compartment to prevent condensation on the cuvette. T_m data were determined as the maxima of the first order derivative of the melting curves and were shown to correspond within $\pm 1^\circ\text{C}$ to those determined at half of the maximal hypochromicity after base line correction.

The CD spectra over 210 nm to 300 nm were recorded on Jasco J720 A spectropolarimeter linked to a IBM PC compatible computer and using a water-jacketed cell holder and cell of 10 mM path length. The temperature of the

samples was kept within an accuracy of $\pm 0.5^\circ\text{C}$ during each spectral measurement using Haake P3 water bath. Each UV and CD spectrum reported was an average of at least ten scans for CD and at least five scans for T_m measurements.

Stock solutions of YR12 and RY12 were prepared having identical molar strand concentration ($30\ \mu\text{M}$) in 10 mM Na-cacodylate, 300 mM NaCl and 10 mM MgCl_2 (pH 5.2). $50\ \mu\text{l}$ aliquots of one oligonucleotide solution was added stepwise to $400\ \mu\text{l}$ of stock solution of the other oligonucleotide contained in a stoppered cuvette¹⁷. After each addition, the cuvette was inverted repeatedly to ensure complete mixing followed by heating at 90°C for one minute, followed by incubation at room temperature for about 20 min and inverting the cuvette again. Absorbance was then recorded at 260 nm and the results given are the average of three absorbance measurements at a particular molar ratio.

UV derivative melting curves of RY12, YR12 and their 1 : 1, 1 : 2 and 2 : 1 molar mixtures at pH 5.2 are shown in Figure 2. Both RY12 and YR12 oligonucleotides show identical melting curves with identical T_m ($43 \pm 1^\circ\text{C}$). 1 : 1 molar mixture of RY12 and YR12 under the same solution condition, on the other hand, shows a biphasic melting profile of a major species with T_m of $38 \pm 1^\circ\text{C}$ and a very minor melting species with $73 \pm 1^\circ\text{C}$. We assign the lower T_m to the melting of the interacting heteroduplex (possibly PS-DNA) which is 5°C lower than that of the T_m of individual homoduplexes. A minor population of a high melting species is clearly discernible in the same mixture, which can be due to hairpin structures. At pH 7.5, however, the same 1 : 1 mixture of the oligomers exhibits melting transition ($T_m = 43 \pm 1^\circ\text{C}$) identical with the melting curves of antiparallel duplexes (data not shown) of the individual oligomers.

Figure 3 shows the CD spectra of RY12 or YR12 alone and their 1 : 1 molar mixtures at room temperature (26°C) and also at 65°C . 1 : 2 and 2 : 1 molar mixture of RY12 and YR12 are also shown in this figure. Room temperature CD spectra (left panel) of all the mixtures at pH 5.2 show distinctive maxima and minima. YR12 and RY12 mixture in the ratio of 1 : 2 shows very intense maxima and minima indicating strong complexation. The characteristic minima at 213 nm is a signature of a triplex structure¹⁸. We have already shown that a triplex is formed by interaction of a single strand of YR12 with a hairpin oligomer (RY28) having the stem of RY12 duplex joined by a –CTTC– loop on one end¹⁵. The 1 : 1 and 1 : 2 molar mixture of RY12 and YR12 on the other hand, exhibit similar spectra of less intensity with a characteristic sharp minima at 213 nm.

CD spectra of these mixtures at 65°C , where the normal antiparallel individual duplexes of RY12 and YR12 are not stable are shown in the right panel of Figure 3. The pattern of CD spectra of the mixtures is seen as that observed at room temperature but with much reduced amplitude. The strong negative peak of the 1 : 1 complex at 213 nm disappeared at this temperature.

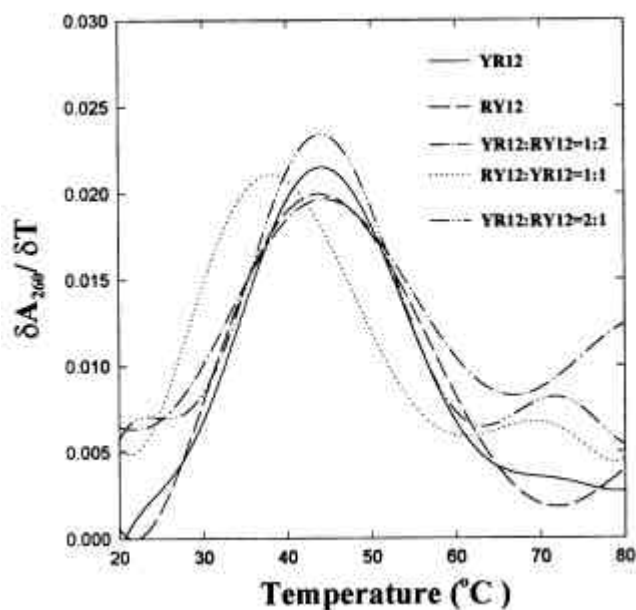


Figure 2. Derivative melting profiles of deoxyoligonucleotides, YR12, RY12 and their mixtures obtained by UV spectroscopy in 10 mM Na-cacodylate, 300 mM NaCl and 10 mM MgCl_2 (pH 5.2).

Figure 4 shows the UV absorbance changes at 260 nm induced by successive addition of RY12 oligonucleotide to YR12 oligonucleotide solution and vice versa in the buffer at pH 5.2, while keeping the total oligomer concentration constant. First-order regression of the data points obtained gives an inflection point around 0.5 mole fraction ratio, in terms of strand concentration of RY12 oligonucleotide, demonstrating formation of a 1 : 1 complex.

Oligonucleotides were designed in such a way that they could form Watson–Crick duplex as well as a perfectly matched parallel duplex with Hoogsteen pairing under appropriate conditions. Stable parallel duplexes have been shown to be formed in either PolyPu–PolyPy sequences or those with exclusively A–T base pairs. Here we show that alternate blocks of purine and pyrimidine bases, which can form antiparallel triplexes with alternate strand pairing^{13,19}, could also lead to parallel duplex formation under appropriate conditions.

As both the oligomers are palindromic in nature, they individually form a perfect Watson–Crick duplex DNA (APS–DNA) in a buffer of pH 5.2, shown by well-defined and overlapping melting curves of each of these dodecamers, having the same T_m values of $43 \pm 1^\circ\text{C}$. When the above two oligomers were mixed in a molar ratio of 1 : 1, heated to 90°C for 2 min and then slowly annealed down to room temperature, the melting curve changed with a shift of 5°C in T_m (38°C) (Figure 2). As T_m of PS–DNA is slightly lower than that of APS–DNA, we thought of the possibility of formation of a parallel DNA structure between YR12 and RY12 under the solution condition.

CD spectra of RY12 and YR12 individually show normal B DNA pattern of Watson–Crick duplex structure. Other oligomer mixtures at 1 : 1 or 1 : 2 ratio show CD spectra different from these individual spectra. The mixtures had a

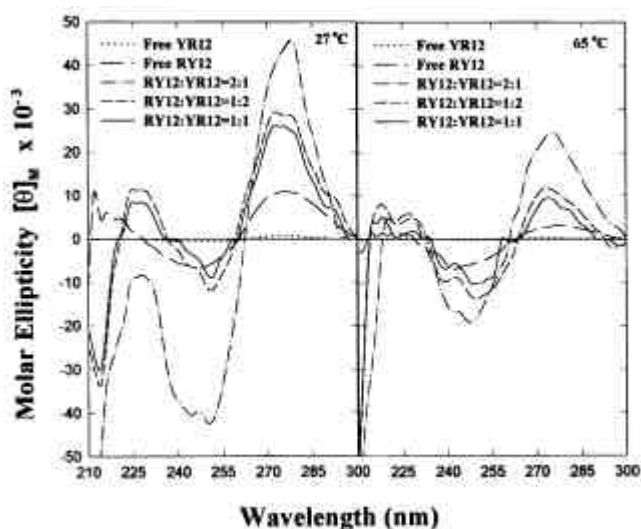


Figure 3. CD spectra of the same oligonucleotide solutions presented in Figure 1 are shown at room temperature (27°C) and at a higher temperature (65°C).

molar ellipticity higher than that of the algebraic sum of the individual molar ellipticities, indicating strong interaction between YR12 and RY12. The 1 : 1 molar mixture at pH 5.2 has a moderate positive band at 274 nm, weak positive band at 227 nm, weak minima at 250 nm and a strong signature minima at 213 nm indicating the formation of a parallel duplex⁹. Interestingly, 1 : 2 and 1 : 1 mixtures of RY12 and YR12 show very similar CD spectra. Liu *et al.*⁹ have shown that spectra of a parallel duplex, and a triplex of which the putative duplex is a component part show remarkably similar CD spectra at pH 5.0 and only differ in intensity.

At 65°C , where the Watson–Crick or Hoogsteen duplexes are expected to denature, we still find that the observed ellipticity of the 2 : 1 complexes (RY12 : YR12) was much higher than the algebraic sum of the individual molar ellipticities. On the other hand, the CD profiles for mixtures of 1 : 2 (RY12 : YR12) and 1 : 1 molar ratios, are only slightly higher than the algebraic sum of the individual molar ellipticities. These results corroborate with the melting curves (Figure 2) in the sense that the 2 : 1 mixture (RY12 : YR12) has a considerable population of high melting species even at 65°C . The 1 : 1 and 1 : 2 mixtures of RY12 : YR12 also have some residual structure, possibly even at 65°C . UV mixing curve determines the stoichiometry of interaction between YR12 and RY12 to be 1 : 1, which indicates the formation of a parallel duplex (Figure 4). The surprising observation is that 1 : 1 and 1 : 2 mixtures of RY12 and YR12 have very similar CD spectra, which are very different in amplitudes from that of the triplex in 2 : 1 mixture of RY12 and YR12. Previously it was shown that while RY12 Watson–Crick duplex can accommodate smoothly a single

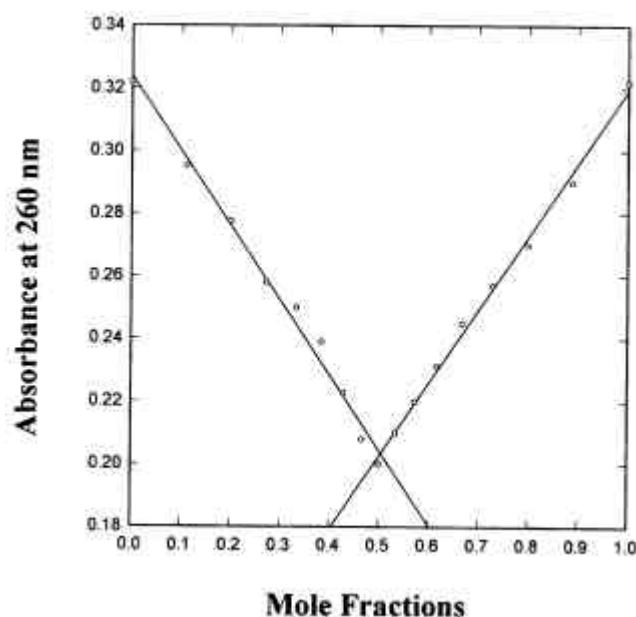


Figure 4. UV mixing curve for the stoichiometry of the complex formed between the interacting RY12 and YR12 oligonucleotides in 10 mM Na-cacodylate, 300 mM NaCl and 10 mM MgCl_2 (pH 5.2). Values in abscissa are the mole fractions of YR12.

strand of YR12 in the major groove to form a triplex with alternate strand pairing, YR12 duplex cannot form such a triplex with a single strand of RY12 (ref. 13). Furthermore, it is known that alternate strand pairing may not be feasible for certain 5'-(Py)_m.(Pu)_n-3' target sequences¹⁹. Several studies have shown that triplex formation at 5'-(Py)_m.(Pu)_n-3' sequences (producing a R triplex followed by a Y triplex) occurs less efficiently than triplex formation at 5'-(Pu)_m.(Py)_n-3' sequences (producing a Y triplex followed by a R triplex)^{20,21}. Thus, it is possible that in a 1 : 2 mixture of RY12 and YR12 a triplex does not form efficiently, instead a mixture of parallel duplex RY12 : YR12 and antiparallel YR12 duplex results upon annealing at room temperature.

1 : 1 stoichiometry of interaction between RY12 and YR12 oligomers suggests a parallel duplex formation with Hoogsteen base pairing at pH 5.2; our UV and CD data are consistent with this view. Liu *et al.*⁹ have shown that a stable parallel double helix with Hoogsteen pairing can exist independently of the triple helix of which it is a component part. We have previously reported intermolecular triplex formation between a hairpin oligomer (RY28) having the stem of RY12 duplex and CTTC loop and a single strand of YR12 but not with RY12. In this context, it is very likely that RY12 and YR12 sequences which are perfectly matched for parallel duplexes with Hoogsteen pairs would form such a duplex. Liu *et al.*⁹ showed that Hoogsteen bonding in A-T and G-C⁺ pairs can easily be made isomorphous by slight rotation of the backbone. Consequently, the A-T and G-C⁺ pairs can in principle be interchanged in any order and the helix may have any base composition. A stereochemical model for such parallel DNA has also been reported²². This perfectly matched parallel duplex between 20 mer homopurine/homopyrimidine strands was stable only below pH 6.0, which rearranged to an imperfectly paired Watson-Crick duplex with looped-out bases when the pH was raised above 6.0. An NMR study²³ on a 1 : 1 mixture of homopurine and homopyrimidine dodecamers of sequences similar to that of Liu *et al.*⁹ and perfectly matched for Hoogsteen base paired parallel duplex, however, failed to detect any such duplex even at pH 4.5. Instead the system was found to prefer antiparallel duplex with mismatches at neutral pH which disproportioned into a triplex with a free purine strand at acidic pH.

Our oligonucleotides are not homopurine or homopyrimidine sequences, instead they contain alternate blocks of purines and pyrimidines. Such sequences with exclusively A-T pairs were the first example to show formation of a parallel DNA structure with reverse Watson-Crick base pairing which were slightly less stable than normal antiparallel B-form helix over a range of pH. Our PS-DNA has a T_m only 5°C lower than corresponding Watson-Crick APS-DNA and is relatively A-T rich. This suggests that base pairing here would also be of reverse Watson-Crick type, but it is stable at pH 5.2, when the cytosines are protonated. A G-C⁺ pair with reverse Watson-Crick bonding is not possible and a slipped Watson-Crick would

not be iso-structural with Donohue-type A-T pairs. In view of pH-dependent protection of N7 of dG residues and other considerations, Pulleyblank *et al.*²⁴ suggested a structure for protonated d(TC)_n.d(GA)_n sequence where dA-dT Watson-Crick base pairs alternate with Hoogsteen ^{SY}dG.dCH⁺ pairs, which was shown to be the most stereochemically acceptable structure consistent with the observed chemical property of the protonated APS-DNA. It may be noted that reverse Hoogsteen bonded dG.dCH⁺ pairs are more iso-structural with reverse Watson-Crick A-T base pairs than are the Hoogsteen ^{SY}dG.dCH⁺ pairs with Watson-Crick A-T base pairs. Preliminary attempts at modelling indicate that A-T pairs with reverse Watson-Crick hydrogen bond can be accommodated with the G-C⁺ pairs with reverse Hoogsteen bonds in the same double helix. In view of these observations we conclude that RY12 and YR12 in 1 : 1 mixture form a parallel DNA at pH 5.2, where the G-C⁺ base pairs are hydrogen bonded in reverse Hoogsteen fashion and the A-T pairs have reverse Watson-Crick hydrogen bonds.

The parallel duplex with Donohue pairs has only a single H-bond between guanine N1 and cytosine N3, which is prevented in case the cytosine N3 are protonated; consequently, parallel duplexes with reverse Watson-Crick base pairs are confined to exclusively A-T pairs. The parallel duplex proposed here has only 5°C lower T_m than corresponding Watson-Crick duplex which suggests that this parallel duplex is also formed with reverse Watson-Crick base pairs, but it is not clear why a Hoogsteen paired PS-DNA does not form in our system. We conclude here that RY12 and YR12 in acidic condition (pH 5.2) form a parallel duplex structure with reverse Watson-Crick base pairing in A-T pairs, and reverse Hoogsteen hydrogen bonding in G-C⁺ base pairs. A schematic drawing of this is given in Figure 5. At neutral pH this parallel-stranded DNA

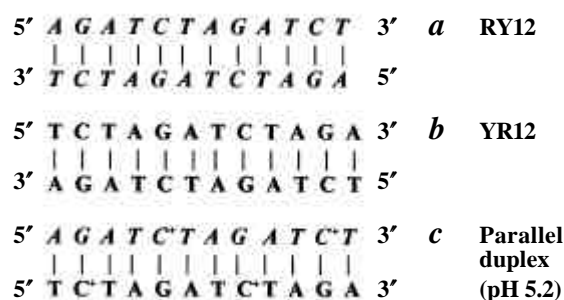


Figure 5. Schematic drawing for antiparallel duplex of *a*, RY12 (italics); *b*, YR12 (bold); and *c*, proposed parallel duplex between RY12 and YR12.

rearranges to form usual antiparallel duplexes of individual dodecamers, since the T_m is raised to $43 \pm 1^\circ\text{C}$ at pH 7.5.

1. Jovin, T. M., Rippe, K., Ramsing, N. B., Klement, R., Elhorst, W. and Vojtiskova, M., in *Structure and Methods: DNA and*

RNA (eds Sarma, R. H. and Sarma, M. H.), Adenine Press, Schenectady, New York, 1990, vol. 3, pp. 155-174.

- van de Sande, J. H., Ramsing, N. B., Germann, M. W., Elhorst, W., Kalisch, B. W., von Kitzing, E., Pon, R. T., Clegg, R. C. and Jovin, T. M., *Science*, 1988, **241**, 551-557.
- Rippe, K., Ramsing, N. B., Kement, R. and Jovin, T. M., *J. Biomol. Struct. Dyn.*, 1990, **7**, 1199-1209.
- Germann, M. W., Kalisch, B. W. and van de Sande, J. H., *Biochemistry*, 1988, **27**, 8302-8306.
- Rippe, K., Ramsing, N. B. and Jovin, T. M., *Biochemistry*, 1989, **28**, 9536-9541.
- Rippe, K. and Jovin, T. M., *Biochemistry*, 1989, **28**, 9542-9549.
- Klysik, J., Rippe, K. and Jovin, T. M., *Biochemistry*, 1990, **9**, 9831-9839.
- Klysik, J., Rippe, K. and Jovin, T. M., *Nucleic Acids Res.*, 1991, **25**, 7145-7154.
- Liu, K., Miles, T. H., Frazier, J. and Sasisekharan, V., *Biochemistry*, 1993, **32**, 11802-11809.
- Fritzsche, H., Akhebat, A., Taillandier, E., Rippe, K. and Jovin, T. M., *Nucleic Acids Res.*, 1993, **21**, 5085-5091.
- Rippe, K., Fritsch, V., Westhof, E. and Jovin, T. M., *EMBO J.*, 1992, **11**, 3777-3786.
- Takeshi, S., Yukio, M., Hitoshi, A. and Ryo, K., *Nucleic Acids Res.*, 1995, **23**, 3771-3777.
- Saha, T. and Roy, K. B., *J. Bioch. Mol. Biol. Biophys. USA*, 1998, (in press).
- Atkinson, T. and Smith, M., in *Oligonucleotide Synthesis: A Practical Approach* (ed. Gait, M. J.), IRL Press, Oxford, England, 1984.
- Pharmacia, Sweden, Gene Assembler Special/4 Primers, Users Manual, Edition AB.
- Banerjee, A., Bose, H. S. and Roy, K. B., *Biochromatography*, 1991, **11**, 650-656.
- Plum, G. E., Park, Y. W., Singleton, S. F., Dervan, P. B. and Breslauer, K. J., *Proc. Natl. Acad. Sci. USA*, 1990, **87**, 9436-9440.
- Antao, P., Gray, M. D. and Ratliff, R. L., *Nucleic Acids Res.*, 1988, **16**, 719-738.
- Jayasena, S. D. and Johnston, B. H., *Biochemistry*, 1993, **32**, 2800-2807.
- Beal, P. A. and Dervan, P. B., *J. Am. Chem. Soc.*, 1992, **12**, 1470-1478.
- Jayasena, S. D. and Johnston, B. H., *Biochemistry*, 1992, **31**, 320-327.
- Raghunathan, G., Miles, H. T., Sasisekharan, V., *Biopolymers*, 1994, **34**, 1573-1581.
- Bhaumik, S. R., Chary, K. V., Govil, G., Liu, K. and Miles, H. T., *Nucleic Acids Res.*, 1995, **23**, 4116-4121.
- Pulleyblank, D. E., Haniford, D. B. and Morgan, A. R., *Cell*, 1985, **42**, 271-280.

ACKNOWLEDGEMENTS. This work was supported by the DST (SP/SO/D39/93). T.S. is thankful to CSIR for the financial support and to Prof. Faizan Ahmad, Department of Biosciences, JMI, New Delhi, for his guidance and encouragement.

Received 20 March 1999; revised accepted 2 June 1999

Partial characterization of goat brain proteins involved in bilirubin binding

Mohd. Mushahid Khan* and Saad Tayyab

Interdisciplinary Biotechnology Unit, Aligarh Muslim University, Aligarh 202 002, India

In order to characterize in terms of bilirubin binding, major proteins in the goat brain were separated into five different peaks, namely P₀, P₁, P₂, P₃ and P₄ on a Seralose-6B column (90.5 × 2.5 cm). The peak P₀ was eluted with the void volume of the column. The molecular weights and Stokes radii of the remaining peak proteins were: P₁ (1,06,727 and 4.11 nm), P₂ (59,256 and 3.25 nm), P₃ (18,713 and 1.71 nm) and P₄ (11,928 and 1.14 nm). Bilirubin binding studies indicated that three out of the five peak proteins, namely P₁, P₂, and P₃ showed bilirubin binding as characterized by the blue shift and hyperchromism in the visible absorption spectra and quenching of the protein fluorescence upon addition of bilirubin to these peak proteins.

HYPERBILIRUBINEMIA is an important pathological condition in the newborn and the possibility of low grade brain damage due to bilirubin toxicity is of interest to clinicians¹. Decreased albumin binding capacity, increased bilirubin concentration or low albumin levels, can account for increased bilirubin deposition in the brain thus leading to the development of the clinical syndrome, kernicterus which may result in infant death². Bilirubin neurotoxicity may be mediated by a number of mechanisms due to its increased permeability in neuronal membranes. Recently, it was reported that the high neonatal serum bilirubin levels adversely affected hearing³, while in newborn piglets its prolonged infusion modified the N-methyl-D-aspartate (NMDA) receptor/ion channel complex in the cerebral cortex⁴. In spite of extensive research, the mechanisms of bilirubin toxicity in the brain and characterization of the bilirubin binding proteins remain elusive. In this paper, we report our data on the characterization of some bilirubin binding proteins in goat brain.

Fresh goat brain, obtained from a local slaughterhouse, was dissected and made free of membranous tissues and

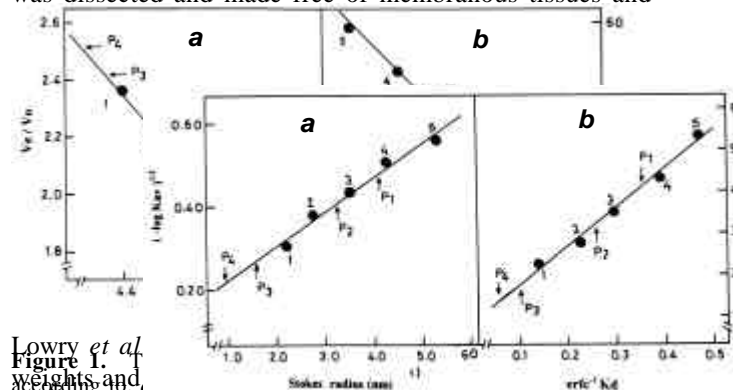


Figure 1. SDS-PAGE gel showing protein bands labeled P₀, P₁, P₂, P₃, and P₄. The gel is divided into two panels, a and b. Panel a shows a molecular weight marker on the left with values 2.6, 2.4, 2.2, 2.0, 1.8, and 1.6. Panel b shows a Stokes radius marker on the left with values 4.4, 4.0, 3.6, 3.2, 2.8, 2.4, 2.0, 1.6, and 1.2. Arrows in both panels point to the positions of the five protein peaks.

*For correspondence. (e-mail: btisamua@nde.vsnl.net.in)

Fresh bilirubin solution was prepared by dissolving few of its crystals in 5 mM NaOH solution containing 1 mM EDTA and diluting it to the desired volume with 0.06 M sodium phosphate buffer, pH 8.0. The concentration of bilirubin was determined spectrophotometrically using a molar extinction coefficient of $47,500 \text{ M}^{-1} \text{ cm}^{-1}$ at 440 nm (ref. 10). Binding of bilirubin to different fractions of goat brain proteins was studied using both visible absorption spectroscopy and fluorescence quenching. Visible absorption spectra of free bilirubin and a complex of bilirubin with different goat brain proteins were recorded in the wavelength range 380–510 nm. All the binding studies were performed in 0.06 M sodium phosphate buffer, pH 8.0, ionic strength 0.15. The molar ratio of bilirubin to protein was kept as 1 : 1 and the spectra were recorded 20 min after adding the desired amount of stock bilirubin solution to the protein solution. Bilirubin binding was also studied by the fluorescence quenching method after adding increasing amount of stock bilirubin solution to a fixed amount of protein solution. The molar ratios between bilirubin and proteins were fixed as 0.0, 0.5, 1.0, 1.5 and 2.0. The final volume was adjusted to 5 ml by adding desired amount of 0.06 M sodium phosphate buffer, pH 8.0, ionic strength 0.15. The fluorescence emission spectra were recorded in the wavelength range of 300–450 nm by exciting the protein at 280 nm. The slit width was 2 nm and 5 nm for the excitation and emission spectra, respectively.

Five distinct peaks, namely P_0 , P_1 , P_2 , P_3 and P_4 were obtained when goat brain homogenate was passed on a Seralose-6B column ($90.5 \times 2.5 \text{ cm}$). The peak P_0 was eluted with void volume of the column. Of the remaining four peaks, P_1 seemed to have higher molecular size followed by P_2 and P_3 , whereas P_4 had the lowest (Figures 1 and 2). Treatment of gel filtration data of marker proteins as well as different proteins of goat brain according to Andrews⁶ and Porath⁷ (see Figure 1 *a, b*) yielded the following straight line equations.

$$V_e / V_0 = 4.92 - 0.58 \log M, \quad (1)$$

$$M^{1/3} = 223.11 - 205.65 Kd^{1/3}. \quad (2)$$

To determine the Stokes radius, gel filtration data were also treated according to Laurent and Killander⁸ and Ackers⁹ which fit the following straight line equations (see Figure 2 *a* and *b*).

$$(-\log K_{av})^{1/2} = 0.08 \text{ Stokes radius} + 0.14, \quad (3)$$

$$\text{Stokes radius} = 9.22 \text{ erfc}^{-1} Kd + 0.84. \quad (4)$$

The values of molecular weights (from equations (1) and (2)) and Stokes radii (from (3) and (4)) for different goat brain

proteins calculated from these equations are listed in Table 1.

Visible absorption spectrum of bilirubin showed an absorption maxima at 440 nm. Addition of different goat brain proteins to the bilirubin solution shifted its absorption maxima to the blue region and enhanced the absorbance (Figure 3 *a*). Occurrence of a blue shift and enhancement in the absorbance of bilirubin solution upon addition of different goat brain proteins were indicative of the binding of bilirubin to these proteins. Similar type of blue shift and enhancement was also observed with different tryptic and

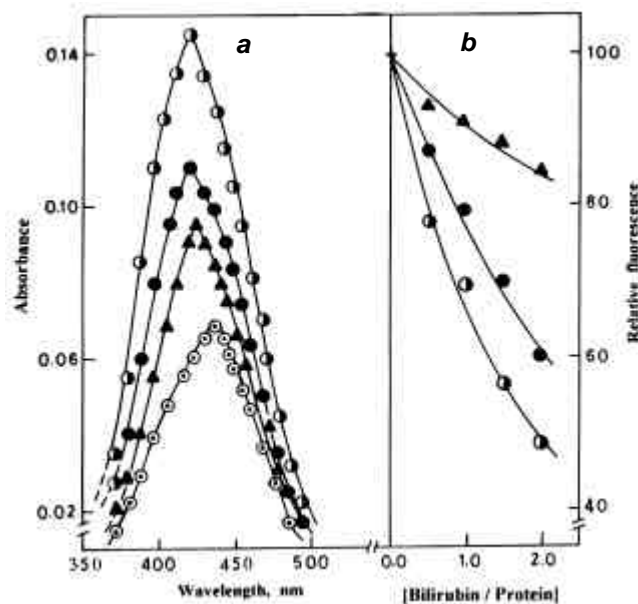


Figure 3. *a*, Visible absorption spectra of bilirubin in the absence and presence of different peak proteins of goat brain. The spectra are: (○) free bilirubin, (●) P_1 + bilirubin, (□) P_2 + bilirubin, and (▲) P_3 + bilirubin; *b*, Fluorescence quenching results of different peak proteins of goat brain at different bilirubin to protein molar ratios. The molar ratios are: 0.0, 0.5, 1.0, 1.5 and 2.0. Different peak proteins are: (○) P_1 , (□) P_2 , and (▲) P_3 .

peptic fragments of serum albumin upon their interaction with bilirubin¹¹. Although these protein fractions were qualitatively similar in terms of bilirubin binding, they varied in terms of the extent of blue shift as well as the magnitude of absorbance. A blue shift of 20 nm was observed with peak proteins P_1 and P_2 , whereas P_3 showed a blue shift of only 15 nm. On the other hand, increase in absorbance was maximum with P_2 followed by P_1 and minimum with P_3 . Peak P_4 did not show any indication of bilirubin binding with this method.

All the three peak proteins, P_1 , P_2 and P_3 gave the fluorescence spectra in the wavelength range 300–450 nm with the emission maxima at 330–334 nm. Addition of bilirubin to these proteins caused quenching in their emission spectra. The bilirubin-induced fluorescence quenching was suggestive of the binding of bilirubin to

RESEARCH COMMUNICATIONS

Table 1. Molecular weights and Stokes radii of different peak proteins of goat brain obtained from gel filtration results at pH 7.0 and ionic strength 0.15

Peak elution volume V_e (ml)	Molecular weight		Stokes radius (nm)	
	From eq. (1)	From eq. (2)	From eq. (3)	From eq. (4)
330	1,03,276	1,10,178	4.11	4.10
355	57,069	61,443	3.25	3.24
400	19,647	17,770	1.59	1.82
415	13,237	10,619	0.91	1.37

these proteins as observed earlier with serum albumin¹². Bilirubin binding to these proteins was studied at different molar ratios between bilirubin and protein and the results were plotted as relative fluorescence against bilirubin to protein molar ratio (Figure 3 b). As is evident from the figure, maximum quenching was observed with peak P₂ at all molar ratios studied, followed by P₁, whereas peak P₃ showed relatively little quenching. Taken together, the data on bilirubin-induced fluorescence quenching and blue shift and enhancement in the visible absorption spectroscopic results suggested that all the three proteins bind bilirubin to a significant extent. Studies are in progress to characterize these proteins in detail in terms of bilirubin binding.

- Hansen, T. W. R. and Bratlid, D., *Acta Paediatr. Scand.*, 1986, **75**, 513–522.
- Brodersen, R., *Crit. Rev. Clin. Lab Sci.*, 1979, **11**, 305–399.
- Ozcelik, T., Onerci, M., Ozcelik, U., Aksoy, S. and Seannaroglu, L., *Acta Otorhinolaryngol. Belg.*, 1997, **51**, 31–34.
- Hoffman, D. J., Zanelli, S. A., Kubin, J., Mishra, O. P. and Delivoria-Papadopoulos, M., *Pediatr. Res.*, 1996, **40**, 804–808.
- Lowry, O. H., Rosenbrough, N. J., Farr, A. L. and Randall, R. J., *J. Biol. Chem.*, 1951, **193**, 265–275.
- Andrews, P., *Methods Biochem. Anal.*, 1970, **18**, 1–53.
- Porath, J., *J. Pure Appl. Chem.*, 1963, **6**, 233–244.
- Laurent, T. C. and Killander, J., *J. Chromatogr.*, 1964, **14**, 317–330.
- Ackers, G. K., *J. Biol. Chem.*, 1967, **242**, 3237–3238.
- Jacobsen, J. and Wennberg, R. P., *Clin. Chem.*, 1974, **20**, 783–789.
- Reed, R. G., Feldhoff, R. C., Clute, O. L. and Peters, T. Jr., *Biochemistry*, 1975, **14**, 4578–4583.
- Tayyab, S. and Qasim, M. A., *Biochim. Biophys. Acta*, 1987, **913**, 359–367.

ACKNOWLEDGEMENTS. Facilities provided by the Aligarh Muslim University, Aligarh are gratefully acknowledged. M.M.K. is a Senior Research Fellow of the Council of Scientific and Industrial Research, New Delhi, India.

Received 5 February 1999; revised accepted 17 April 1999

Somatic instability for chlorophyll pigmentation in cotton (*Gossypium* spp.)

R. Sheshagiri and B. M. Khadi

Agricultural Research Station, Dharwad Farm, Dharwad 580 007, India

Since centuries, variegated plants have been identified and preserved by man as ornamentals. The phenomenon of variegation is also observed in crop plants. In the present study, chlorophyll mosaics were identified and scored in various cotton populations. All four cultivated *Gossypium* species and their hybrids showed variegation, but high frequency of mosaics were seen in cytoplasmic male sterile (CMS) lines. The variegation was either limited to a leaf or branch or expressed throughout the plant. Various patterns of yellowing were observed on leaves, bractioles and bolls. The possible mechanisms involved in creation of such somatic instability are discussed, which can have implications in cotton genetics, breeding and biotechnology.

AMONG the living organisms, the phenomenon of variegation; the unusually spotted, striped, or otherwise mosaic appearance of some individuals as opposed to their normally uniform counterparts, has long been a source of fascination. In plants, variegation, very often ascribed to somatic instability, is most easily recognized as irregularities in pigment patterns on leaves, flowers and seeds. Researchers hope that variegation may contribute to our understanding of an organism's capacity for change and provide a starting point for unraveling the complex mechanisms underlying its development¹. Analysis of somatic chlorophyll mutants has been a useful tool for the study of either spontaneous^{2,3} or induced^{4,5} genetic instability-related phenomena in plants.

Cotton (*Gossypium* spp.) is an important fibre crop of the world. Among the four cultivated species of *Gossypium* grown in India, *G. arboreum* and *G. herbaceum* are diploids and known as Desi cottons. The other two species, viz. *G. hirsutum* and *G. barbadense* are tetraploids and known as New world cottons. In our breeding programmes, (though it failed earlier to catch our attention), in the past few years we often encountered one or two cotton plants exhibiting yellow and/or white spots/stripes on green leaves. Such chlorophyll mosaic plants were observed commonly in varietal/hybrid trails and in crossing blocks. To understand the pattern of variegation and to know their frequencies, all the available breeding populations sown during Kharif 1998 were persistently screened for occurrence of the mosaic plants, at various plant developmental stages.

In a broad sense, the material screened in the study consisted of (i) varieties of four cultivated species of *Gossypium*; (ii) inter-specific hybrids among two diploids

(*G. arboreum* × *G. herbaceum*) and two tetraploids (*G. hirsutum* × *G. barbadense*); (iii) intra-specific *hirsutum* hybrids; and (iv) male sterile (MS) lines involving both cytoplasmic (CMS) and genetic (GMS) male sterility systems. The number of genotypes screened under each category and the number of plants scored for each genotype are presented along with the frequencies of chlorophyll mosaic plants in Table 1. In general, around 50 or more genotypes were considered in each population except for *G. arboreum* varieties (24), inter-specific diploid hybrids (9) and GMS lines (4). One hundred plants were scored for each genotype except for *G. barbadense* varieties (10) and inter-specific diploid hybrids (50).

As is evident from Table 1, all the cotton populations studied invariably had few chlorophyll mosaic plants. Out of the 736 genotypes screened, 177 genotypes (24.05×10^{-2}) yielded 330 mosaic plants (0.50×10^{-2}). In general, the frequency of unstable genotypes was more in male sterile lines (65.57×10^{-2}) followed by intra *hirsutum* hybrids (31.23×10^{-2}), *Gossypium* varieties (13.7×10^{-2}) and the inter-specific hybrids (9.17×10^{-2}). Though relatively less numbers of genotypes were screened, *G. arboreum* exhibited highest instability (45.8×10^{-2}) among the four species, followed by *G. hirsutum* (27.2×10^{-2}). The low frequency (2.4×10^{-2}) observed in *G. barbadense* may be due to the less number of plants scored, which can be supported by the moderate frequency (0.24×10^{-2}) observed on a whole population basis. However, *G. herbaceum* was distinctly stable with only two genotypes (2.5×10^{-2}) showing mosaics. Among the inter-specific hybrids, both the diploids (11.10×10^{-2}) and tetraploids (9.00×10^{-2}) had almost similar frequencies of unstable lines. In the intra *hirsutum* hybrids, CGMS-based hybrids (56.30×10^{-2}) dominated for instability and interestingly the conventional intra *hirsutum* hybrids (22×10^{-2}) almost maintained the trend of *hirsutum* varieties (27.2×10^{-2}). Among the male sterile lines, though GMS lines showed higher frequencies (75×10^{-2}) of unstable lines, it may have less implications as only four GMS lines were screened. However, the CMS lines exhibited a very high level (64.9×10^{-2}) of instability for chlorophyll pigmentation which was the maximum among any population screened in the present study followed by the CGMS-based hybrids.

The population frequencies (Table 1) further confirmed the higher instability of the CMS lines and the CGMS-based hybrids as they recorded 1.44×10^{-2} and 1.11×10^{-2} , respectively at the population level. Infact, 179 (54%) of the 330 mosaic plants isolated in the present study were contributed only by these two populations. Among the four *Gossypium* species, the frequency of mosaic plants was maximum for *G. arboreum* varieties (1.08×10^{-2}) and minimum (0.02×10^{-2}) for *G. herbaceum*, indicating its inherent stability. All other populations maintained moderate frequencies between 0.2 and 0.4×10^{-2} except the GMS-based hybrids (0.75×10^{-2}). Table 1 also indicates that among the genotypes, in general, the frequency of mosaic

RESEARCH COMMUNICATIONS

plants ranged up to 7×10^{-2} except for the varieties of *G. herbaceum* and *G. barbadense* (1×10^{-2}), GMS lines (1×10^{-2}) and the inter-specific diploid hybrids (2×10^{-2}). However, a very high level of instability was noticed in one conventional hirsutum hybrid (DHH-156) with a frequency of mosaics as high as 12×10^{-2} .

The relationship between CMS and high frequency of chlorophyll mosaics was further confirmed through another study. In a crossing block, 10 plants of 64 CMS lines (known as A lines) were grown along with 10 plants of their corresponding B (male fertile) lines to be used as pollen parents for the maintenance of A lines. When all the plants were scored, 1–2 mosaic plants were seen in 14 A lines, however there was a single mosaic plant in only

one B line. To analyse this phenomenon in detail, 100 plants of 24 A lines (which are extensively used in crossing programmes) and their corresponding B lines were scored for the occurrence of chlorophyll mosaics (data not shown). Mosaics were found in 15 A lines (frequency, 62×10^{-2}) at a population frequency 1.4×10^{-2} , whereas only 5 B lines (20.8×10^{-2}) showed mosaics in a frequency of 0.21×10^{-2} which is much lower compared to the A lines.

Closer examination of the mosaic plants revealed interesting details about the variegation. In few plants, a single leaf was chimeric, while in others variegation was restricted to one monopodial branch. The lateral sides of the upper half of a few plants were chlorophyll-deficient but in others the upper half was completely yellow. There were also cases in which the variegation was distributed all over

Table 1. Frequency of chlorophyll mosaic plants in various cotton populations

Sl. no.	Population	No. of genotypes screened	No. of plants scored in each genotype	No. and frequency of genotypes showing mosaics		No. of plants scored in each population	No. and frequency of mosaics in each population		Range of frequencies of mosaic plants among genotypes ($\times 10^{-2}$)
				Number	Frequency ($\times 10^{-2}$)		Number	Frequency ($\times 10^{-2}$)	
Varieties of different <i>Gossypium</i> species									
1.	<i>G. herbaceum</i>	81	100	2	2.5	8100	2	0.02	1
2.	<i>G. arboreum</i>	24	100	11	45.8	2400	26	1.08	1 to 5
3.	<i>G. hirsutum</i>	81	100	22	27.2	8100	34	0.42	1 to 7
4.	<i>G. barbadense</i>	84	10	2	2.4	840	2	0.24	1
	Sub total	270	–	37	13.7	19440	64	0.33	1 to 7
Inter-specific hybrids									
1.	<i>G. herb.</i> \times <i>G. arbo.</i> (Diploids)	9	50	1	11.10	450	1	0.22	2
2.	<i>G. hirs.</i> \times <i>G. barb.</i> (Tetraploids)	111	100	10	9.0	11100	13	0.23	2 to 6
	Sub total	120	–	11	9.17	11550	14	0.12	2 to 6
Intra-specific (<i>hirsutum</i> \times <i>hirsutum</i>) hybrids									
1.	Conventional hybrids	150	100	33	22.00	15000	56	0.37	1 to 12
2.	GMS-based hybrids	48	100	7	14.60	4800	14	0.29	1 to 4
3.	CGMS-based hybrids	87	100	49	56.30	8700	97	1.11	1 to 6
	Sub total	285	–	89	31.23	28500	167	0.59	1 to 12
Male sterile lines									
1.	GMS lines	4	100	3	75.00	400	3	0.75	1
2.	CMS lines	57	100	37	64.90	5700	82	1.44	1 to 6
	Sub total	61	–	40	65.57	6100	85	1.39	1 to 6
	Grand total	736	–	177	24.05	65590	330	0.50	1 to 12

GMS – Genetic male sterility, governed by nuclear genes.

CMS – Cytoplasmic male sterility, governed by cytoplasmic genes.

CGMS – Cytoplasmic genic male sterility, wherein CMS could be restored by nuclear genes.

G. herb. – *G. herbaceum*; *G. arbo.* – *G. arboreum*;

G. hirs. – *G. hirsutum*; *G. barb.* – *G. barbadense*.

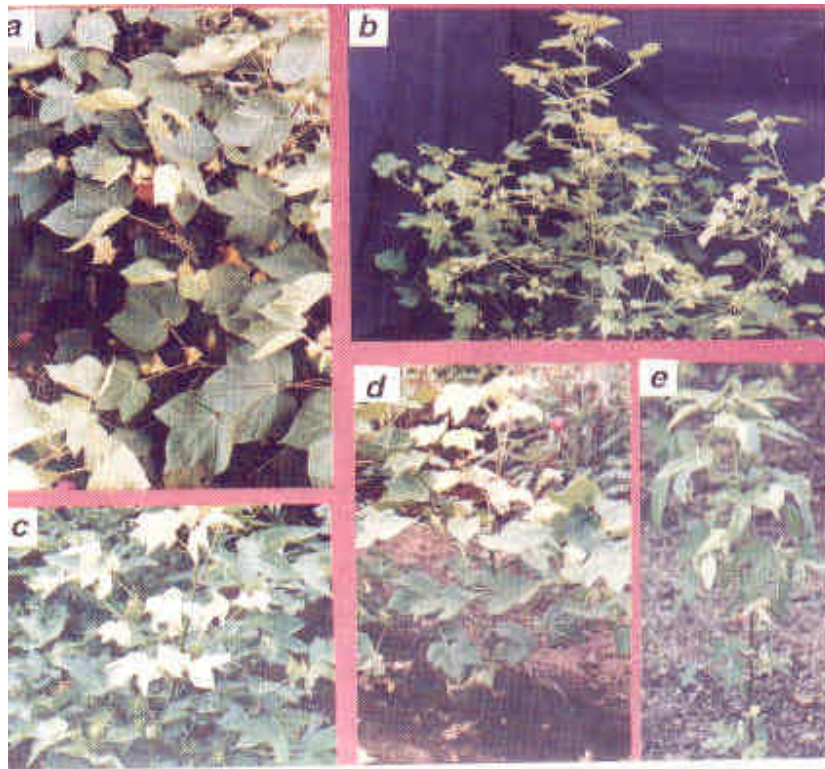


Figure 1. Distribution of variegation in various plant parts. *a*, Single leaf mosaic; *b*, Single monopodial branch mosaic; *c*, A lateral side (towards the viewer) of upper half mosaic; *d*, Upper half completely yellow; and *e*, Whole plant mosaic.

the plant (Figure 1). A wide spectrum of different patterns of variegation was also observed within individual leaves. The leaves had either white/yellow spots/stripes all over or had definite yellow sectors. Few leaves had exactly half yellow portions and some leaves were completely deficient in chlorophyll content (Figures 2 *a–d*). Further, variegation was not only restricted to leaves but extended on to the bractioles and bolls. Bractioles and bolls also exhibited various patterns of yellowing (Figures 2 *e–h*).

Genetic instability was first recorded in plants by Knight⁶ and Emerson⁷. They noted that this instability can be associated with the behaviour of an unstable allele of an otherwise standard locus. McClintock^{8,9} carefully studied the behaviour of a few maize (*Zea mays* L.) lines in generating variegated phenotypes and found that this characteristic was often associated with the activity of mobile DNAs termed controlling, or transposable elements (TEs). In the present study, insertion of such cryptic genetic elements into the genes involved in chlorophyll synthesis must have inactivated the host genes leading to chlorophyll-deficient yellow patches on leaves. Further, their excision in future mitotic divisions resulted in reactivation (known as somatic reversion) of genes and synthesis of chlorophyll, finally exhibiting yellow spots or stripes in a green background. As shown in Figure 1, the distribution of variegation in a particular leaf, monopodial

branch, lateral upper half, upper half or throughout the plant may be indicative of the temporal and spatial differences in the activation of the putative TEs. Similarly the various forms of variegation observed on leaves, bractioles and bolls (Figure 2) might denote the particular point of development of the respective tissue when mutations occurred. Variegation in the form of red stripes and sectors on leaves, flower and pericarp of the seed were noticed in candystripe genotype of sorghum, which was later confirmed to be due to activity of transposons¹⁰. Somatic instability has been proven to be an important tool for studying the fates of developing tissues by somatic sector analysis¹¹.

Further, the present study also indicated a possible role of cytoplasm in creation of genetic instability. This conclusion was made based on two facts, viz. (i) the nuclear genomic constitution of A and B lines remains the same but differ only for their cytoplasm and hence the high frequency of mosaics observed in A lines as compared to B lines may be due to the unstable cytoplasmic genes; (ii) all the CGMS-based hybrids shown in Table 1 had one or the other 24 A lines described later as their female parents. The comparison of the 24 A lines (62×10^{-2}) and the CGMS-based hybrids (56.30×10^{-2}) for the frequency of mosaics exemplifies the possible maternal inheritance of the instability from CMS lines to



Figure 2. *a-d*, Patterns of variegation on leaf. *a*, Yellow/white spots/stripes on leaf; *b*, Yellow sectors; *c*, Half leaf yellow; *d*, Full leaf yellow. *e-h* Patterns of variegation on bractioles and/or bolls. *e*, Yellow spots/stripes; *f*, Yellow sectors; *g*, Half boll yellow; *h*, Full boll yellow.

CGMS hybrids. Existence of the TEs in chloroplast was first postulated by Sears¹² and the recent studies on chlorophyll-deficient mutants of barley¹³⁻¹⁵ have confirmed chloroplast transposon activation under a particular nuclear genotype. McClintock¹⁶ proposed that TEs in an organism get activated when the organism is subjected to genomic stress. In cotton, the CMS lines have been developed with the cytoplasm of a diploid species, *Gossypium herknessii* by transferring the nuclear genome of tetraploid species *G. hirsutum* which must have created such a stress to activate the putative cytoplasmic transposons. However, it needs confirmation through genetic and molecular analyses.

1. Nevers, P., Shepherd, N. S. and Saedler, H., *Adv. Bot. Res.*, 1985, **12**, 103-203.
2. Grandbastien, M. A., *Nestle Res. Newslett.*, 1986/87, pp. 31-45.
3. Kirk, J. T. O. and Tinley-Bassett, R. A. E., in *The Plastids*, Elsevier Publications, Amsterdam, 1978.
4. Constantin, M. J. and Nilan, R. A., *Mutat. Res.*, 1982, **99**, 37-49.
5. Prina, A. R. and Favret, E. A., *J. Hered.*, 1988, **79**, 371-376.
6. Knight, T. A., *Trans Linn Soc. London*, 1808, **XIX**, 9.
7. Emerson, R. A., *Am. Nat.*, 1914, **48**, 87-115.
8. McClintock, B., *Carnegie Inst. Washington Yearb.*, 1948, **47**, 155-169.
9. McClintock, B., *Cold Spring Harbor Symp. Quant. Biol.*, 1956, **21**, 197-216.
10. Zanta, C. A., Yang, X., Axtell, J. D. and Bennetzen, J. L., *J. Hered.*, 1994, **85**, 23-29.
11. Dawe, R. K. and Freeling, M., *Dev. Biol.*, 1990, **142**, 233-245.
12. Sears, B. B., *Stadler Symp.*, 1983, **15**, 119-139.
13. Prina, A. R., in *Barley Genetics VI* (ed. Munck, L.), Muncksgaard International Ltd, Copenhagen, 1991, vol. 1, pp. 316-318.
14. Prina, A. R., *Theor. Appl. Genet.*, 1992, **85**, 245-251.
15. Prina, A. R., *J. Hered.*, 1996, **87**, 385-389.
16. McClintock, B., *Science*, 1984, **226**, 792-801.

ACKNOWLEDGEMENT. We acknowledge Dr M. V. C. Gowda, Genetics and Plant Breeding, University of Agricultural Sciences, Dharwad, for conception of the idea and manuscript preparation.

Received 20 February 1999; revised accepted 10 May 1999

A new seismic hazard map for the Indian plate region under the global seismic hazard assessment programme

M. Ravi Kumar* and S. C. Bhatia

National Geophysical Research Institute, Uppal Road, Hyderabad 500 007, India

A new seismic hazard map for the Indian plate region, comprising the Himalaya, northeast India, the Indian shield, South China, Nepal, Burma and Andaman regions, was prepared under the Global Seismic Hazard Assessment Programme (GSHAP). A working catalogue of main shocks was obtained by merging the local catalogues from different countries, with the global catalogue of NOAA. Eighty-six potential seismic source zones were delineated based on the major tectonic features and seismicity trends. Using the probabilistic hazard assessment approach, the Peak Ground Accelerations (PGA) were computed for 10% probability of exceedence in 50 years, at locations defined by a grid of $0.5^\circ \times 0.5^\circ$. The PGA values over the grid points were contoured to obtain a seismic hazard map. The map reveals that the zones of highest risk are the Burmese arc, northeastern India and the Hindukush regions, with PGA values of the order of 0.35–0.4 g. Also, a majority of the north Indian plate boundary region and the Tibetan plateau region have a hazard level of the order of 0.25 g. In the Indian shield region, it is of the order of 0.05–0.1 g, whereas some locales like Koyna depict a hazard level of about 0.20 g.

SEISMIC hazard, in the context of engineering design, is generally defined as the predicted level of ground acceleration which would be exceeded with 10% probability at the site under consideration, in the next 50 years, due to the occurrence of an earthquake anywhere in the region. A lot of complex scientific perception and analytical modelling is involved in seismic hazard estimation. A computational scheme essentially involves delineation of seismic source zones and their characterization, selection of an appropriate ground motion attenuation relation and choosing a predictive model of seismic hazard.

Since earthquake catalogues constitute the first essential input for the delineation of seismic source zones and their characterization, preparation of a unified working catalogue for a region under consideration is an important task. Globally, the data from historic times to recent can be broadly divided into three temporal categories: (1) from 1964 till recent, for which modern instrumentation-based data are available; (2) from 1900–1963, the era of early instrumental data; and (3) pre-1900, consisting of pre-instrumental data, based primarily on historical and macro-seismic information. The next key component of seismic hazard assessment is the creation of seismic source models,

which demand translating seismotectonic information into a spatial approximation of earthquake localization and temporal recurrence. The seismotectonic maps need to be critically studied for defining areal seismic source zones and active faults. An earthquake recurrence model is then fitted to these source zones for defining the parameters that characterize the seismicity of the source region, which go as inputs to the algorithm for the computation of seismic hazard, viz. minimum and maximum magnitudes and the parameters a and b in the earthquake frequency magnitude relationship $\log N = a - bM$. The third main element required for seismic hazard assessment is the designation of the strong ground motion (ground acceleration) estimation equations, specifying the ground acceleration as a function of earthquake magnitude and hypocentral distance. These equations have been developed for only a few regions of the world. Obtaining realistic estimates of strong ground motions in all regions is a major challenge that must be met.

Although the steps involved in hazard assessment are specific to the region under consideration, certain standardization of the approaches is essential so that estimates can be compared worldwide and their consistency ensured across the regional boundaries. Global Seismic Hazard Assessment Programme (GSHAP) is a programme which has been coordinated internationally and implemented at the regional and local levels through a number of centers. It has adopted the probabilistic hazard assessment approach of McGuire to estimate the Peak Ground Accelerations (PGA) using the FRISK88M software. Each center has been responsible for a defined geographical territory for the preparation of a unified/homogeneous earthquake catalogue, compilation of seismo-tectonic information and earthquake source delineation, strong seismic ground motion studies and the computation of predictive seismic hazard. The National Geophysical Research Institute (NGRI), Hyderabad, India was identified as one such center, responsible for estimating the seismic hazard for the Indian region.

The issue of seismic hazard in India had been addressed by scientists as early as 1956 when a 3-zone (severe, moderate, minor hazard) seismic zoning map of India was brought out¹. This map was based on a broad concept of earthquake distribution and geotectonics. The severe hazard zones were roughly confined to plate boundary regions, i.e. the Himalayan Frontal Arc in the north, the Chaman fault region in the northwest and the Indo-Burma border region in the northeast. While the minor hazard zone was confined to the Indian shield region in the south, the moderate hazard zone covered the transitional zone between the two. Since then many versions of the seismic zoning map of India have been brought out. The Bureau of Indian Standards, which is the official agency for publishing seismic hazard maps and codes in India, prepared a six-zone map in 1962, a seven-zone map in 1966, and a five-zone map in 1970/1984 which is currently valid. The present five-zone

*For correspondence. (e-mail: postmast@csngri.ren.nic.in)

map is under review. Khattri *et al.*² adopting a probabilistic hazard computational approach, published a map of, seismic hazard in units of 'g', for 10% probability of exceedence in 50 years.

The present study was initiated during an international workshop of the GSHAP, held at NGRI in February–March 1996. The study region comprised the Test Area #8 of GSHAP, covering parts of India, China, and Nepal, bounded by 20°N–40°N and 85°E–105°E. Towards the preparation of an earthquake catalogue for source zonation, the NOAA catalogue and several local catalogues were considered. A working catalogue of main shocks was prepared by removing duplicates, aftershocks and earthquakes without any magnitude. To start with, the test area was divided into 16 source zones on the basis of seismicity patterns emerging from a plot of epicenters in the region in conjunction with the tectonic information. Further exercises were subsequently carried out with 30 source zones and 56 source zones. After a critical examination of the seismicity and tectonic constraints along with the computed PGA values, it was felt that the 30-source zone model was best suited for the region³.

Subsequently, the study was extended to a larger region bounded by 0–40°N and 65–100°E, which included the entire Himalayan belt, northeast India, the Indian shield, South China, Nepal, Burma and Andaman regions.

To delineate the source zones based on seismicity and tectonic information, a compilation of the tectonic features of the Indian region was made (Figure 1), based on a generalized tectonic map of India², tectonic map of the Himalayan Arc⁴, tectonic map of India published by the Oil and Natural Gas Commission, sketch map of major tectonic features of southeast Asia⁵, map of the Tibetan region showing fault plane solutions of moderate earthquakes and active faults⁶ and some unpublished material. Figure 2a shows the seismicity map of the study region for earthquakes of magnitude 4 and above. Figure 2b shows the earthquakes of magnitude 6 and above, to highlight regions which have experienced major earthquakes in the past. As can be seen, the seismicity of the Indian region is intense along its plate margins and is rather diffused in other regions, except for some concentrations in regions like Koyna. The tectonic and seismicity patterns of the Indian plate boundary regions have been studied in detail using a large number of focal mechanism solutions of the Harvard CMT data^{7–9}. Based on the seismicity and tectonic trends, 86 potential source zones were delineated (Figure 2a, b), which are described here.

The boundaries of the Indian plate are characterized by a continental collision segment along the Himalaya in the north, a complex to an oblique subduction along the Burma–Andaman arc in the east and transverse fault systems such as the Chaman fault in the northwest. It is now well known that the continued northward collision of the Indian plate with respect to the Eurasian landmass is the source of intense seismicity, and has produced the most

gigantic topographic features of the world, viz. the Himalaya and the Tibetan plateau. The major tectonic features in this region include, from south to north, the Main Boundary Thrust (MBT), the Main Central Thrust (MCT) and the Indus Tsangpo Suture Zone (ITSZ). These linear tectonic features run all along the Himalayan belt from west to east having a NW–NS trend in the northwestern Himalaya, E–W trend in the western, central and eastern Himalaya and NE–SW trends in the northeastern Himalaya.

Most of the seismicity in the Himalayan region is concentrated along shallow north dipping planes, which indicate underthrusting of the Indian plate beneath the Eurasian plate. In addition to the four great earthquakes of magnitude exceeding 8 during 1897, 1905, 1934 and

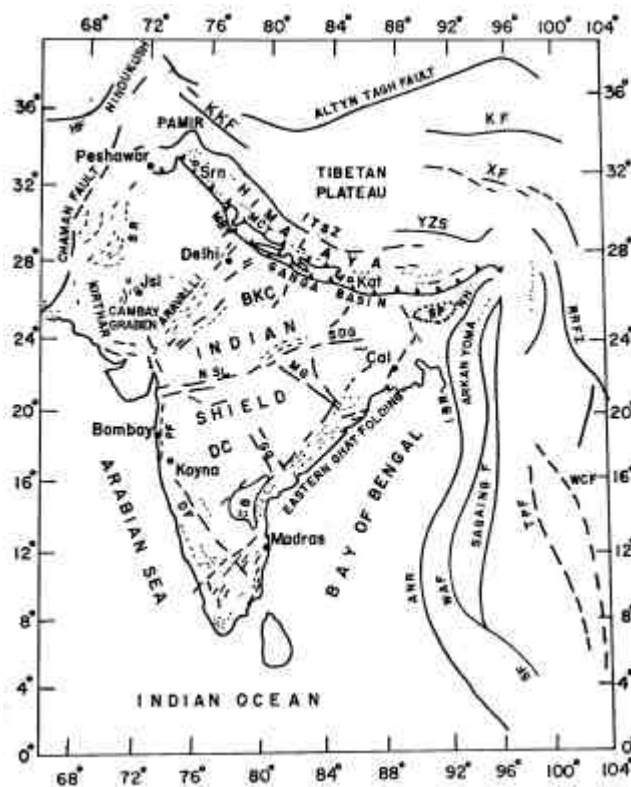


Figure 1. Generalized tectonic map of India and adjoining regions. Abbreviated Tectonic features are: ANR, Andaman Nicobar Ridge; CB, Cuddapah Basin; DF, Dharwar Fold; GG, Godavari Graben; HF, Herat Fault; IBR, Indo-Burma Ranges; ITSZ, Indus Tsangpo Suture Zone; KF, Kunlun Fault; KKF, Karakoram Fault; MBT, Main Boundary Thrust; MCT, Main Central Thrust; MG, Mahanadi Graben; SDG, Satpura Damodar Graben; NH, Naga Hills; NSL, Narmada–Son Lineament; PF, Panvel Flexure; RRFZ, Red River Fault Zone; SF, Sagaing Fault; SR, Sulaiman Range; SP, Shillong Plateau; TPF, Three Pagodas Fault; WAF, West Andaman Fault; WCF, Wang Chao Fault; XF, Xian Shui He Fault; YZS, Yarlung Zangpo Suture. Cities shown are: Cal, Calcutta; Jsl, Jaisalmer; Kat, Kathmandu; Srn, Srinagar.

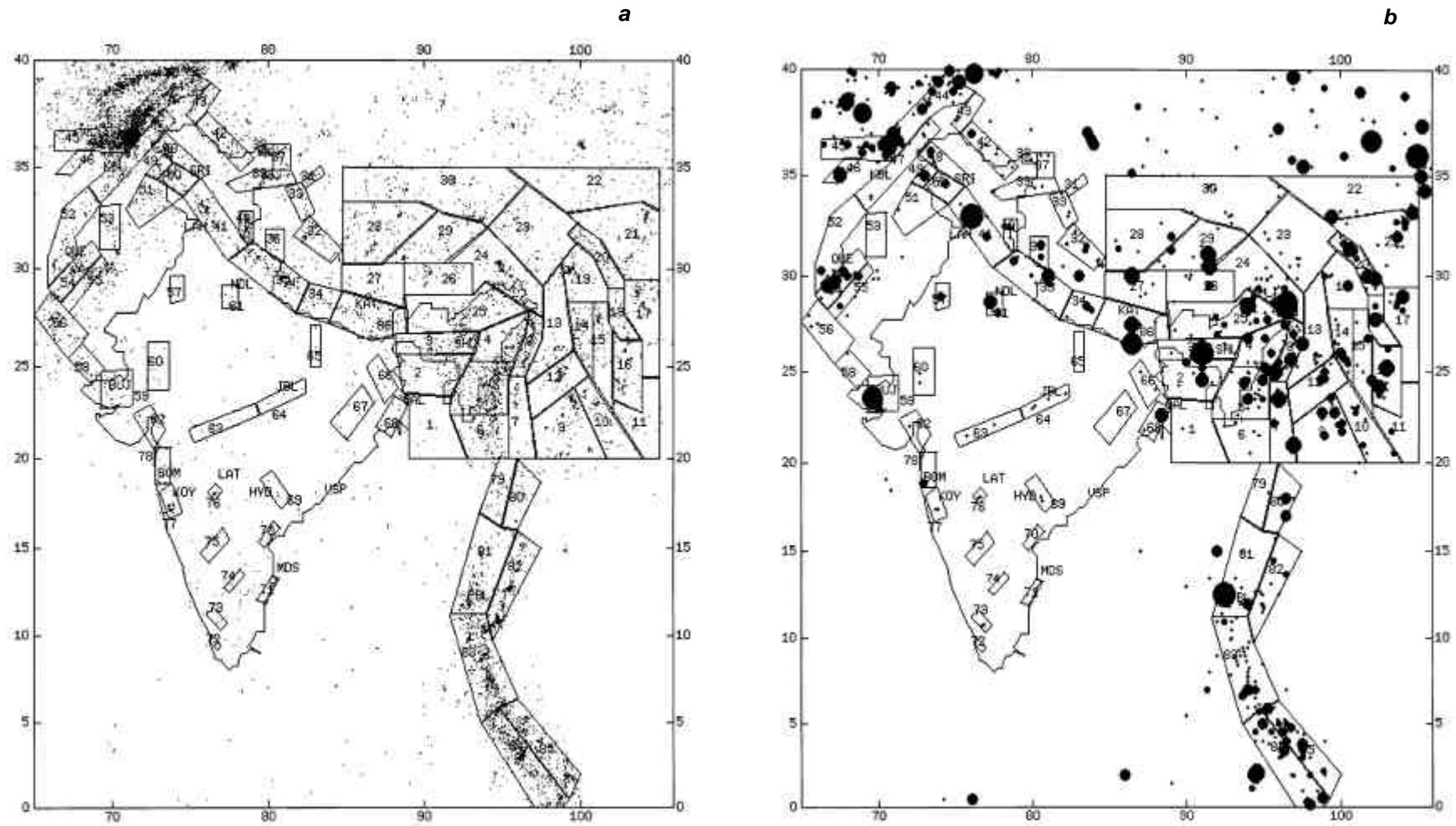


Figure 2. *a*, Seismicity and source zone map of India and adjoining regions. Dots are the epicenters of earthquakes of magnitude 4 and above. Blocks numbered 1 through 86 are the source zones. Some cities are shown for orientation purpose: BMB (Bombay), BUJ (Bhuj), CAL (Calcutta), HYD (Hyderabad), JBL (Jabalpur), KAT (Kathmandu), KBL (Kabul), KOY (Koyna), LAH (Lahore), LAT (Latur), MDS (Madras), NDL (New Delhi), PBL (Port Blair), QUE (Quetta), SHL (Shillong), SRI (Srinagar), VSP (Vishakhapatnam). *b*, Map showing locations of earthquakes of magnitude 6 and above in India and adjoining regions. Three letter locations refer to cities as listed in the caption of Figure 2 *a*.

1950, another 10 earthquakes exceeding magnitude 7.5 have occurred in the Himalayan belt during the past 100 years. From a very simple consideration, the whole Himalayan belt, from west to east, can be considered as one seismic-source zone. However, dividing the zone into smaller segments would be more appropriate. We have therefore segmented this region by source numbers 25 and 86 in the eastern sector, sources 34 through 36 in the central sector, 40 and 41 in the western sector and 37 through 39, 42, 48 through 50 in the northwestern sector.

In contrast to thrusting in the Himalaya, the extraordinarily thick crust of the Tibetan plateau in the north is characterized by crustal extension and eastward extrusion, manifested by earthquakes indicating normal faulting and strike-slip motion. The Altyn Tagh, the Kunlun and the Xianshuihe are the three major fault systems supporting the left-lateral strike-slip motion⁶. Sources 22 through 24, and 26 through 33 have been delineated in this zone based primarily on seismicity trends (Figure 2 *a*).

The Burma–Andaman arc marks the eastern margin of the Indian plate, along which an oblique convergence between the Indian and the Burmese plate has been suggested^{10,11}. The major tectonic features along the arc are the N-S trending Indo-Burman Ranges (IBR) in the north and the Andaman Nicobar Ridge (ANR) in the south. The Sumatran fault system in the southeast, the Western Andaman Fault (WAF) and the Sagaing fault further east, are the features supporting major right lateral movements in this region. The distribution of earthquakes in the Burmese arc region suggests the presence of a subducted Indian lithospheric slab beneath the Burmese plate^{12–15}. Occurrence of shallow and intermediate focus earthquakes has been reported in the Naga Hills (NH), and Arakan Yoma fold belt⁸. While the seismic source zones 4 through 8 cover the Burmese arc and adjoining region on the eastern side, the source zone 3 on the west encompasses the Shillong Plateau (SP) which experienced a strong earthquake of magnitude 8.7 in 1897. The tectonics of the Shillong plateau is distinctly different from that of the regions to its north, south and west¹⁶, and hence a separate zone for the region. The area further east, namely the south China region is characterized by many faults and lineaments such as Red River Fault Zone (RRFZ). The seismic sources 9 through 23 have been identified in this seismic province.

The nature of convergence varies from a continental type in the Burmese arc to an oceanic type in the Andaman arc, with a relatively quiet seismic zone marking the transition^{8,17}. Shallow and occasional intermediate depth earthquakes delineate the subducted slab under the Andaman Nicobar islands joining the seismicity trend of the Indo-Burman ranges. A distinct, separate lineation of shallow focus earthquakes passes under the Central basin of the Andaman sea and indistinctly follows the line of the Sagaing fault, towards the eastern Himalayan syntaxis¹¹. The transition seismic zone referred above has been divided into sources 79 and 80. In the region south of this, along the

Andaman Nicobar region sources 81 through 83 have been assigned. Further south the sources 84 and 85 cover the northern Sumatra region.

The northwestern Himalayan region also has the characteristic Himalayan tectonic features, namely MBT, MCT and is bordered by the Hindukush syntaxis and the Pamir knot region in the extreme northwest. The Hindukush and Pamir knot region are characterized by the junction of several tectonic features. This plate boundary region experiences high level of seismicity varying from shallow to intermediate depth earthquakes. Sources 43 through 46 cover this region. The other prominent tectonic features in the northwestern Indian region are the transverse fault systems known as the Chaman fault, the Kirthar and Sulaiman Ranges (SR). The tectonics of the Kirthar Ranges and Sulaiman Ranges is influenced by transcurrent faulting. This region also belongs to the plate boundary and experiences a high level of seismicity. These areas are covered by sources 47, and 51 through 55.

The Indian shield region is marked by several rift zones and shear/thrust zones. Although considered to be a stable continental region (SCR), it has experienced many earthquakes of magnitude $M \geq 6.0$ since the 18th century¹⁸, some of which were disastrous. Among them are the Mahabaleshwar (1764), Kutch (1819), Damooh hill (near Jabalpur, 1846), Mount Abu (1848), Coimbatore (1900), Son-Valley (1927), Satpura (1938), and Jabalpur (1997) earthquakes. The spatial distribution of these moderate earthquakes is shown in Figure 2 *b*. The seismicity in the shield region is quite diffused except for a few localized alignments, which is detailed in this figure. Generally speaking, the Indian shield region can be considered as one single seismic source zone for hazard computations. However, smaller seismic zones can be delineated in this region, primarily based on the locales of the major earthquakes and seismic lineaments, some of which are not so well defined. Next, we describe the nature of seismicity, tectonic trends and the distribution of seismic sources.

The Narmada–Son Lineament (NSL) is a prominent tectonic feature of the Indian shield, trending ENE-WSW from 21°N, 72°E on the western coast of India to 24°N, 88°E on the eastern side. This apparently divides the shield into 2 sectors, which we name as the northern and the southern sectors, to facilitate further description and discussion. The Narmada–Son region has been experiencing earthquakes of different magnitudes in the past, the recent one being the 21 May 1997 Jabalpur earthquake of magnitude 6.0. This is an SCR earthquake with an unusual focal depth of about 30 km. At least 4 earthquakes of magnitude > 5.4 have earlier occurred along this zone, two of them in the proximity of the 1997 Jabalpur earthquake¹⁹. We have assigned 2 probable seismic zones in the central part of the Narmada–Son lineament numbered 63 and 64. Further, while the northeast portion of the Indian shield is covered by sources 66 through 68, the region west of the Burmese arc and south of the Shillong plateau is described by sources 1 and 2.

The major tectonic constituents in the southern sector of the Indian shield include the massive Deccan Volcanic Province (DVP), the South Indian Granulite Terrain (SIGT), the Dharwar Craton (DC), the Cuddapah Basin (CB), the Godavari Graben (GG), the Mahanadi Graben (MG), and the Eastern and the Western Ghats on the east and west coast of India, respectively.

The Eastern ghat region in general is a quiet zone, characterized by diffused low magnitude shallow focus earthquakes and an occasional earthquake of magnitude 5–6. The preferred fault plane solutions generally indicate NE–SW orientation with left lateral strike-slip motion. An alternate set of solutions indicate thrust faulting along northwest orientation. Not very many historical earthquakes are reported to have occurred in this region. Based on localized concentration of seismicity, we have delineated sources 70, 71 and 74 along the Eastern Ghat region.

The western ghat region of the Indian shield also depicts diffused seismicity, except for some clusters, the prominent one being the Koyna–Warna region. The Koyna reservoir region has been experiencing induced earthquakes right from the date of its first filling in 1962. Over the past 34 years, the region around the reservoir has experienced 10 earthquakes of magnitude ≥ 5 , over 100 earthquakes of magnitude ≥ 4 , and about 100,000 earthquakes of smaller magnitudes. The world's largest reservoir-induced earthquake of magnitude 6.3 occurred in the Koyna region on 10 December 1967. Warna reservoir located 20 km south of Koyna began to be filled in 1986. The Koyna–Warna region has experienced a burst of seismicity since August 1993. More than thousand earthquakes of magnitude around 2–3 have occurred since then. Two earthquakes of magnitude 5 and 5.4 occurred on 8 December 1993 and 1 February 1994 respectively. Gupta *et al.*²⁰ and Rai *et al.*²¹ give a detailed picture of seismicity in the Koyna–Warna region. The seismicity in the region aligns itself beautifully along the local/regional fault systems. This Koyna–Warna region does assume a special relevance from the seismic hazard point of view. This region therefore has been considered as a separate seismic source zone numbered 77. The region along the western coast, north of Koyna has been considered as two sources, 78 and 62.

The source 78 around Mumbai is characterized by N–S tectonic lineaments such as the Panvel Flexure (PF) and similarly aligned seismicity patterns. This source region is also reported to have experienced a large earthquake in historic times. The source 62 encompasses the NW–SW trending features in the Cambay Basin and the western end of W–E trending Narmada–Son lineament also depicts reasonable level of seismicity to merit designation of an independent seismic source. Down south, near Trivandrum along the western margin we have delineated source 72 primarily on account of some recent concentration of seismic activity.

In the central shield region south of the Narmada–Son

lineament the seismic activity is considerable, although diffused. The Latur region in central India experienced an earthquake of M_w 6.1 in 1993. The inferred depth was about 5 km and the focal mechanism by several agencies indicated a thrust type faulting with the P axis trending NNE, consistent with the direction of the India–Eurasia plate motion. The inferred fault plane was strikes along the NW and dips 45 degrees SW. Seeber *et al.*²² suggested that the earthquake was caused by a new fault in the Deccan trap region. On the other hand, Rajendran *et al.*²³ inferred the trend of a pre-existing fault based on a study of Landsat images prior to the earthquake. On the basis of borehole studies across the fault, which indicate large displacement of 3 to 6 m, Gupta *et al.*²⁴ suggested that the displacement is far too much to be accounted by a single earthquake of M_w 6.1 and concluded that the fault is a pre-existing one. It appears that this region has also been active in historical times. In view of these considerations, the region around Latur has been taken as a seismic source zone numbered 76. The source 69 covers the Godavari Graben (GG) region which experienced a moderate-sized earthquake of magnitude 5.3, known as Bhadrachalam earthquake, in 1969. The regions around Bellary and Coimbatore have been demarcated as source zones 75 and 73, respectively on account of having experienced moderate-sized earthquakes in the past, as referred in the earlier section.

The northern sector of the Indian shield has relatively lower level of seismicity. The region has a prominent tectonic feature called the Bundelkhand Craton (BC) in the central area bounded by NNE–SSW to N–S trending lineaments on the west as well as on the east. Sources 57, 60, 61 and 65 are delineated in this region.

The northwestern corner of the Indian shield (in the vicinity of 24°N and 72°E) is characterized by N–S, NW–SE and E–W tectonic trends and shows a relatively higher level of seismicity. Sources 56, 58 and 59 have been identified in this region. The source zone 59 experienced the well-known 7.8 magnitude Kutch earthquake in 1819.

To facilitate the steps for source zone characterization, a software toolbox was developed, which performs the essential data handling and pre-processing tasks: (1) scanning of earthquake catalogues (of different formats) to segregate events for the specified rectangular block defined by latitude–longitude limits, or a polygonal block defined by latitudes and longitudes of the vertices; (2) merging different catalogues and sorting in chronological order; (3) removal of duplicates; (4) removal of aftershocks according to a defined criteria and preparation of a main-shock catalogue; (5) plotting of epicenters by superposing the source zones and tectonic features, geographical locations, etc.; (6) estimation of a and b values; and (7) extracting required information from the output files of FRRISK88M, for preparation of hazard maps.

Table 1. Characteristics of the seismic source zones

Source no.	Max. magnitude	Nu (at mag. 5.0)	Beta	Source no.	Max. magnitude	Nu (at mag. 5.0)	Beta
1	6.5	0.016	1.379	44	8.0	3.385	1.610
2	8.5	0.378	1.194	45	8.5	1.434	1.549
3	8.7	0.422	1.449	46	7.5	0.042	1.549
4	8.5	0.566	1.134	47	7.5	0.689	1.617
5	8.5	1.712	1.134	48	7.0	0.150	1.649
6	8.0	0.482	1.570	49	7.5	0.089	1.671
7	8.0	0.201	1.130	50	7.0	0.104	1.671
8	8.0	0.591	1.340	51	7.0	0.151	1.919
9	7.0	0.416	1.008	52	8.0	0.205	1.771
10	7.0	0.602	1.068	53	7.0	0.079	1.634
11	7.0	0.172	1.263	54	7.5	0.349	1.668
12	7.5	0.243	1.062	55	7.5	0.154	1.634
13	6.5	0.352	1.139	56	7.0	0.074	1.795
14	7.5	0.410	1.445	57	7.0	0.001	1.379
15	7.5	0.287	1.268	58	7.5	0.011	1.266
16	8.5	0.353	1.071	59	8.5	0.126	1.266
17	7.0	0.383	1.278	60	6.5	0.034	1.379
18	7.5	0.192	1.387	61	7.5	0.026	1.379
19	7.5	0.221	1.219	62	6.5	0.049	1.379
20	8.0	0.285	1.219	63	6.5	0.034	1.379
21	7.5	0.487	1.292	64	6.5	0.022	1.379
22	8.0	0.199	1.421	65	6.0	0.008	1.379
23	7.0	0.422	1.432	66	6.5	0.001	1.379
24	8.5	0.704	1.253	67	6.0	0.039	1.379
25	8.5	0.864	1.073	68	6.5	0.028	1.379
26	8.0	0.270	0.979	69	6.5	0.033	1.379
27	8.5	0.133	1.495	70	6.0	0.050	1.379
28	8.0	0.494	1.362	71	6.0	0.006	1.379
29	8.0	0.426	0.997	72	6.0	0.008	1.379
30	7.0	0.739	1.308	73	6.0	0.016	1.379
31	6.5	0.247	1.394	74	6.0	0.001	1.379
32	7.0	0.164	1.394	75	6.0	0.006	1.379
33	7.0	0.077	1.394	76	6.5	0.003	1.379
34	8.0	0.171	1.230	77	6.5	0.128	1.379
35	8.0	0.631	1.406	78	6.5	0.128	1.379
36	7.5	0.086	1.406	79	6.5	0.148	1.378
37	7.0	0.143	1.634	80	7.5	0.139	1.378
38	7.0	0.030	1.634	81	8.5	0.694	1.434
39	7.0	0.174	1.764	82	7.0	0.677	1.367
40	7.5	0.155	1.193	83	7.5	1.809	1.361
41	8.5	0.405	1.388	84	7.5	1.676	1.440
42	7.5	0.298	1.323	85	7.5	1.259	1.409
43	7.5	0.069	2.131	86	8.5	0.395	1.495

The minimum magnitude was assigned as 5.0 for all the source zones because it is the lower level of magnitude which would cause hazard of a significant level. The maximum magnitude was estimated from past seismicity for each of the zones separately. The seismic parameters a and b were estimated by applying the maximum likelihood method, and subsequently converted to Nu and Beta, which go as inputs to hazard computations.

The source zones corresponding to the seismically active regions in the plate boundary and adjacent regions contain enough statistics for independent computation of a and b values. However, the source zones in the Indian shield, do not contain sufficient information for this purpose. To overcome this problem, the b value was computed for the whole shield region as one unit and was assigned to each zone within it, while the a value was computed for each zone separately. A similar philosophy was adopted for a few other source zones with sparse seismicity. The details of the characteristics of each source zone are listed in Table 1.

Using the probabilistic hazard assessment approach of McGuire adopted by GSHAP, the PGA were computed using the FRISK88M software for 10% probability of exceedence in 50 years, at locations defined by a grid of $0.5^\circ \times 0.5^\circ$ in the region 0°N – 40°N and 65°E – 100°E . Since no reliable estimates of attenuation values are available for the Indian region, the attenuation relation of Joyner and Boore²⁵ was used. The PGA values over the grid were contoured to obtain a seismic hazard map (Figure 3). A contour interval of 0.05 g was chosen, since we believe that problems and uncertainties associated with the source zone definition and paucity of the seismicity information would not permit a resolution better than 0.05 g. The hazard map depicts that a majority of the plate boundary region and the Tibetan plateau region have hazard levels of the order of 0.25 g with prominent highs of the order of 0.35–0.4 g in the seismically active zones like the Burmese arc, northeastern India and northwest Himalaya/Hindukush region. In most of the Indian shield region, the regional seismic hazard is of the

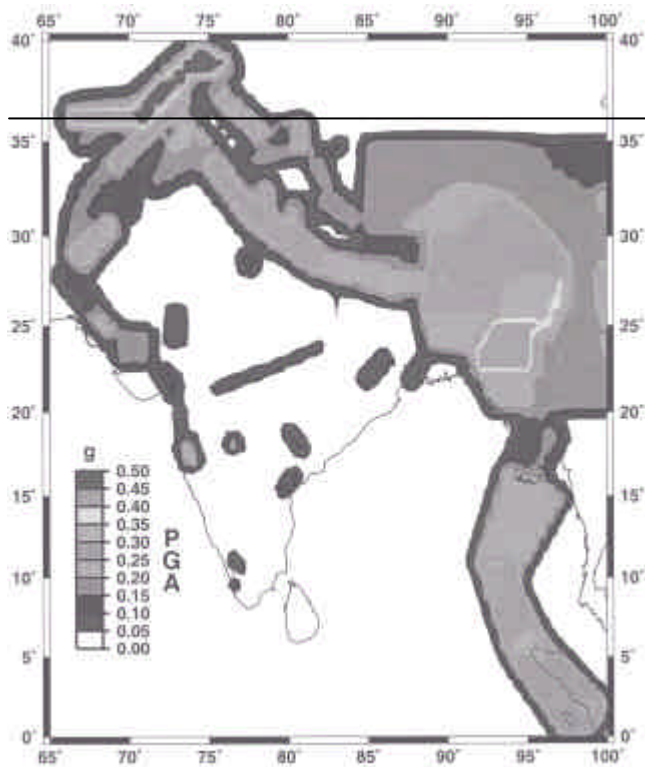


Figure 3. Seismic hazard map of India and adjoining regions for 10% probability of exceedence in 50 years. Contour interval 0.05 g.

order of 0.1 g, whereas some locales like Koyna depict a hazard level of 0.20 g.

The computational experience gained in the GSHAP exercises has brought out certain concerns. The Indian region poses a lot of problems for data homogenization, and seismic hazard maps are strongly influenced by the size and shape of the seismic source zones. Another key issue which is a cause of concern is non-availability of representative strong motion attenuation formulae which compelled us to be satisfied with applying one of the internationally developed formulae. The seismic hazard map of India and adjoining regions presented here is one possible map with all constraints outlined. This map, we believe, gives a reasonably representative seismic hazard picture over the region covered.

We have carried out computations considering the probable source zone depth as 10 km. Any depth shallower than this would be unrealistic since large earthquakes do not take place at very shallow depths. Any depth deeper than 10 km would also not have much meaning because it would reduce the hazard considerably and one needs to take a conservative but realistic approach. The hazard values in the map presented here are lower than the ones given by Khattri *et al.*². We would get the same level of hazard if the source depth was put at 0 km. Apparently Khattri *et al.*² took source depth of 0 km, which produced higher values of hazard estimates.

1. Tandon, A. N., *Indian J. Meteorol. Geophys.*, 1956, **10**, 137–146.
2. Khattri, K. N., Rogers, A. M., Perkins, D. M. and Algermissen, S. T., *Tectonophysics*, 1984, **108**, 93–134.
3. Bhatia, S. C., Gupta, H. K., Ravi Kumar, M., Rao, N. P., Chitraker, G. R., Zhang, P. and Yang, Z-X, Abstract, 29th General Assembly of IASPEI, 18–28 August 1997, Thessaloniki, Greece, p. 387.
4. Khattri, K. N., *Tectonophysics*, 1987, **138**, 79–92.
5. Leloup, P. H., Lacassin, R., Tapponier, P., Schaerer, U., Dalai, Z., Xiaohan, L., Lianshang, Z., Shaocheng, J., Trong and Trinh, P. T., *Tectonophysics*, 1995, **251**, 3–84.
6. Molnar, P., *J. Himalayan Geol.*, 1992, **3**, 43–78.
7. Ravi Kumar, M. and Rao, N. P., *Phys. Earth Planet Inter.*, 1995, **90**, 75–80.
8. Ravi Kumar, M., Rao, N. P. and Chalam, S. V., *Tectonophysics*, 1996, **253**, 155–165.
9. Ravi Kumar, M., Rao, N. P. and Bhatia, S. C., *Curr. Sci.*, 1998, **75**, 311–316.
10. Fitch, T. J., *J. Geophys. Res.*, 1972, **77**, 4432–4460.
11. Curray, J. R., Emmel, F. J., Moore, D. G., Raitt, R. W., Henry, M. and Kieckhefer, R., in *Geological and Geophysical Investigations of Continental Margins* (eds Watkins, J. S., Montadert, L. and Dickerson, P.), AAPG Memoir 1979, **29**, 189–198.
12. Verma, R. K., Mukhopadhyay, M. and Ahluvalia, M. S., *Tectonophysics*, 1976, **32**, 387–399.
13. Mukhopadhyay, M. and Das Gupta, S., *Tectonophysics*, 1988, **149**, 299–322.
14. Ni, J. F., Speziale, M. G., Bevis, M., Holt, W. E., Wallace, T. C. and Seager, W. R., *Geology*, 1989, **17**, 68–71.
15. Gupta, H. K., Fleitout, L. and Froidevaux, C., *J. Geol. Soc. India*, 1990, **35**, 235–250.
16. Rao, N. P. and Ravi Kumar, M., *J. Phys. Earth*, 1997, **45**, 167–176.
17. Chandra, *Tectonophysics*, 1984, **105**, 279–290.
18. Ramalingeswara Rao, B., (personal communication).
19. Gupta, H. K., Chadha, R. K., Rao, M. N., Narayana, B. L., Mandal, P., Ravi Kumar, M. and Kumar, N., *J. Geol. Soc. India*, 1997, **50**, 85–91.
20. Gupta, H. K., Rastogi, B. K., Chadha, R. K., Mandal, P. and Sarma, C. S. P., *J. Seismol.*, 1997, **1**, 47–53.
21. Rai, S. S., Singh, S. K., Sarma, P. V. S. S. R., Srinagesh, D., Reddy, K. N. S., Prakasam, K. S. and Satyanarayana, Y., *Proc. Indian Acad. Sci. (Earth Planet. Sci.)*, 1999, **108**, 1–14.
22. Seeber, L. G., Ekstrom, S. K., Jain, C. V. R., Murthy, Chandak, N. and Ambruster, J. G., *J. Geophys. Res.*, 1996, **101**, B4, 8543–8560.
23. Rajendran, C. P., Rajendran, K. and John, B., *Geology*, 1996, **24**, 651–654.
24. Gupta, H. K., Dwivedi, K. K., Banerji, D. C., Rao, R. U. M., Rao, G. V. and Srinivasan, R., Abstract, Chapman Conference on Stable Continental Region Earthquakes, 25–29 January 1998, NGRI, Hyderabad, 1998, p. 39.
25. Joyner, W. B. and Boore D. M., *Bull. Seismol. Soc. Am.*, 1981, **71**, 2011–2038.

ACKNOWLEDGEMENTS. We thank Dr H. K. Gupta for support and guidance, Dr N. Puranchandra Rao for help in compiling the tectonic map and Dr B. R. Rao for providing his unpublished catalogue of the Indian shield region. The help rendered by Mrs M. Murli Kumari is thankfully acknowledged. We also thank Dr Peizhen Zhang for discussions and collaborative work in the test area and Dr Robin McGuire for providing his s/w package.

Received 13 May 1999; accepted 27 May 1999